Journal of Hydrology 573 (2019) 607–615

Contents lists available at ScienceDirect

Journal of Hydrology

journal homepage: www.elsevier.com/locate/jhydrol

Research papers

Attributing changes in future extreme droughts based on PDSI in China

Jie Zhang[a], Fubao Sun[b,a,c,*], Wenli Lai[d], Wee Ho Lim[a], Wenbin Liu[a], Tingting Wang[a], Pengtao Wang[e]

[a] Key Laboratory of Water Cycle and Related Land Surface Processes, Institute of Geographic Sciences and Natural Resources Research, Chinese Academy of Sciences, Beijing, China
[b] Xinjiang Institute of Ecology and Geography, the Chinese Academy of Sciences, Urumchi, China
[c] Center for Water Resources Research, Chinese Academy of Sciences, Beijing, China
[d] School of Geography and Environmental Science, Hainan Normal University, Haikou, China
[e] School of Tourism & Research Institute of Human Geography, Xi'an International Studies University, Xi'an 710128, China

ARTICLE INFO

This manuscript was handled by Marco Borga, Editor-in-Chief, with the assistance of Sergio M. Vicente-Serrano, Associate Editor

Keywords:
Extreme drought
Global warming
Numerical experiments
Attribution
China

ABSTRACT

Climate change in mean-state or variability could lead to more/less frequency of extreme drought. In this study, we developed a new framework for decomposing the contributing factors of changes in future extreme drought frequency in China in accordance to the Palmer Drought Severity Index (*PDSI*). We performed a series of numerical experiments to ensure that the sensitivity of trend and variability in individual climatic variables can be distinguished. In addition, an extreme drought rate with warming (*EDRW*, unit: $\%\cdot K^{-1}$) is defined to quantify the relative change in extreme drought frequency per Kelvin. Overall, the *EDRW* will increase dramatically by an average of $27.71\%\cdot K^{-1}$. The ascended *EDRW* are attributed to increases in temperature ($+56.90\%\cdot K^{-1}$), net radiation ($14.80\%\cdot K^{-1}$) and precipitation variability ($+8.23\%\cdot K^{-1}$); a decrease in relative humidity ($+4.61\%\cdot K^{-1}$), but is partly offset by an increase in precipitation (i.e., "wetting", $-60.12\%\cdot K^{-1}$). A smaller increase in the frequency of extreme droughts is found in high-latitude regions due to their enhanced sensitivity to "wetting".

1. Introduction

Drought is a major natural hazard that occurs intermittently in many climates (Mishra and Singh, 2010). Measured by the level of water availability below normal conditions over a given period (monthly scale up to multiannual scale), drought severity of a region can be quantitatively assessed using drought indices (i.e., the Palmer Drought Severity Index, *PDSI*, Palmer, 1965, and the Standardized Precipitation Evapotranspiration Index, *SPEI*, Vicente-Serrano et al., 2010). According to drought classifications, extreme (or severe) droughts can be identified when an indicator value falls below a given threshold (e.g., −4 or −3 for *PDSI*) (Palmer, 1965; Kauffman and Vonck, 2011). Because of their serious social-economic consequences (e.g., widespread crop failure or water shortages, Liu et al., 2018a), extreme droughts have gained widespread attentions and discussions, such as the recent California drought (Aghakouchak et al., 2015; Diffenbaugh et al., 2015), the Millennium drought in Southeast Australia (Van Dijk et al., 2013; Kiem et al., 2016) and the once-in-a-century droughts in the southwest China (Qiu, 2010; Zou et al., 2005).

In a climate system that is not subject to adverse impacts of climate change, the frequency of extreme drought could be expected to maintain a relatively stable low probability (Fig. 1a). However, the frequency of extreme droughts are expected to increase as a consequence of the climate change (Dai and Zhao, 2016), and the increase in frequency of extreme drought due to global warming in recent decades was confirmed in many regions (including China) (Zhang et al., 2018). Theoretically, the conditions of sustained drying due to decreasing long-term precipitation and/or increasing evaporation could increase the risk of extreme droughts (Dai and Zhao, 2016; Herrera-Estrada et al., 2017) (Conceptual Model 1 in Fig. 1b). Nonetheless, there is no evidence of an increase in mean-state of drought over China in recent decades (Sheffield et al., 2012; Wang et al., 2015; Zhang et al., 2018; Chen et al., 2017).

The contrasting changes in the mean-state of drought and its extremes can be identified using the increasing volatility of drought with global warming (Zhao and Dai, 2016; Swain et al., 2018; He and Li, 2018). Previous studies highlighted that increased climate variability (i.e., precipitation) could cause more extreme droughts/floods despite

* Corresponding author at: Key Laboratory of Water Cycle and Related Land Surface Processes, Institute of Geographic Sciences and Natural Resources Research, Chinese Academy of Sciences, Beijing, China.
E-mail address: sunfb@igsnrr.ac.cn (F. Sun).

https://doi.org/10.1016/j.jhydrol.2019.03.060
Received 24 October 2018; Received in revised form 13 March 2019; Accepted 15 March 2019
Available online 21 March 2019

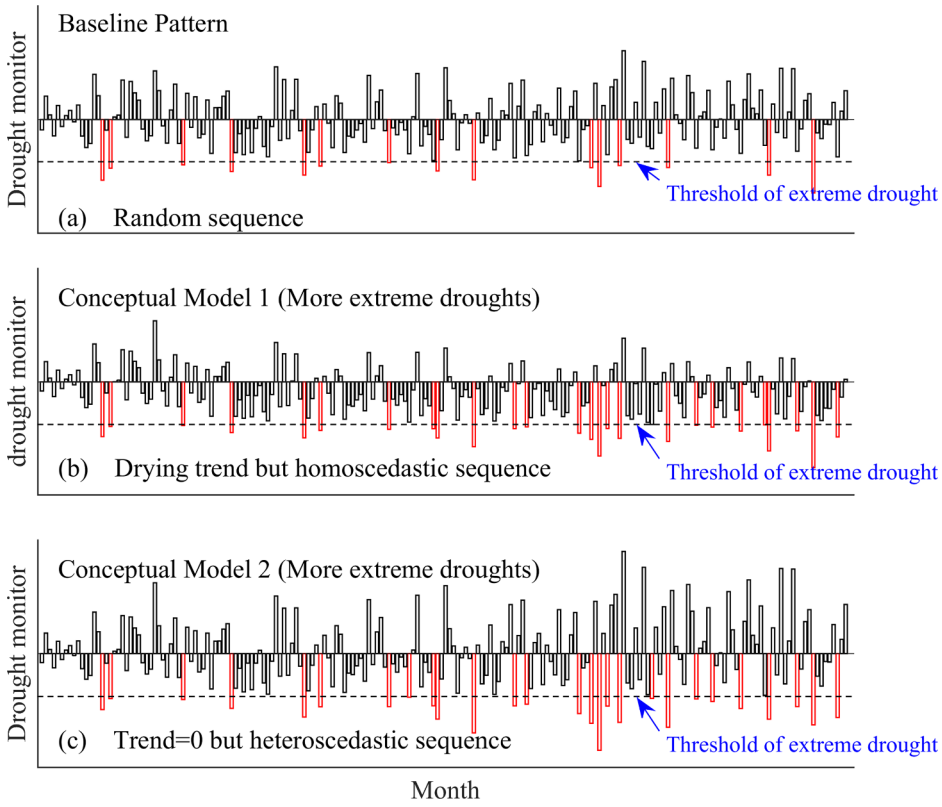

Fig. 1. Conceptual models for explaining the change in extreme drought frequency: (a) baseline pattern without climate change; (b) conceptual model 1 with a decreasing mean state of drought, which predicts more extreme droughts; c) conceptual model 2 with an unchanged mean state of drought but with amplified variability, which predicts more extreme droughts (and more extreme floods).

the change in mean-state is small (Wetherald, 2009; Seager et al., 2012; Chen and Sun, 2015; He and Li, 2018) (Conceptual Model 2 in Fig. 1c). Hence, the projected increase in extreme drought frequency in a warmer world (Prudhomme et al., 2014; Cook et al., 2015; Lehner et al., 2017; Liu et al., 2018b) should be due to the change in mean-state and variability of drought.

However, a quantitative assessment of the sensitivity of future extreme droughts in response to the changes in the mean and variability of various climate variables in a warming climate is not available (He and Li, 2018). To this end, we propose a new framework involving a series of numerical experiments for attributing changes in future extreme droughts across China in accordance to the *PDSI*. In Section 2, we describe the data and design a series of numerical experiments to attribute changes in extreme droughts. In Section 3, we report the assessment and attribution results of projected changes in future extreme drought frequency across China. We present our conclusions and summary in Section 4.

2. Data and methods

2.1. Data

Monthly meteorological variables from the outputs of seven general circulation models (*GCMs*) under the concentration pathway scenario *RCP8.5* (+8.5 W/m^2) (see Table 1 for details) are used in this study. They were archived by the Program on Climate Model Diagnosis at a website that permits downloading (http://pcmdi9.llnl.gov/esgf-web-fe/). The data sets include monthly precipitation (denoted *P*), surface air temperature (maximum, minimum) (denoted *T*), surface relative humidity (denoted *Rh*), net radiation (shortwave downwelling/upwelling flux, Rs_{up}/Rs_{down} and longwave downwelling/upwelling flux Rl_{up}/Rl_{down}, net radiation = $(Rs_{up}\text{-}Rs_{down}) + (Rl_{up}\text{-}Rl_{down})$) (denoted *Rn*), and wind speed. To obtain the monthly wind speed, we averaged the daily values (surface zonal velocity component, *uwnd* and meridional velocity component, *vwnd*, wind speed = $\sqrt{uwnd^2 + vwnd^2}$) over a month (denoted *Ws*). To ensure physical consistency between the climatic variables (Naumann et al., 2018; Liu et al., 2018b), we directly apply the raw climate outputs instead of bias-corrected data. We use the bilinear interpolation to re-grid all GCM climate fields to a common resolution (2° × 2° longitude by latitude) grid.

2.2. Estimating the frequency of extreme drought

The *PDSI* is used in this study to quantify the frequency of extreme drought. It was improved using a simple two-layer water balance model (Palmer, 1965), which considered water supply (i.e., precipitation) and

Table 1
Details of CMIP5 climate models applied in this study.

Climate models	Abbreviation	Modelling groups (Country)	Horizontal resolution
ACCESS1.0	ACCESS	Commonwealth Scientific and Industrial Research Organization/Bureau of Meteorology (Australia)	1.300° × 1.900°
BCC_CSM1.1	BCC	Beijing Climate Center (China)	2.813° × 2.791°
BNU-ESM	BNU	Beijing Normal University (China)	2.810° × 2.810°
CanESM23	CANESM	Canadian Centre for Climate Modelling and Analysis (Canada)	2.813° × 2.791°
IPSL-CM5B-LR	IPSL	Institut Pierre Simon Laplace (France)	1.875° × 3.750°
MRI-CGCM3	MRI	Meteorological Research Institute (Japan)	1.125° × 1.125°
MIROC-ESM	MIROC	Atmosphere and Ocean Research Institute (The University of Tokyo)/ National Institute for Environmental Studies/ Japan Agency for Marine-Earth Science and Technology (Japan)	2.813° × 2.791°

atmospheric evaporative demand. The precipitation used in *PDSI* estimation need to be estimated under climatically appropriate conditions (Zhang et al., 2018; Liu et al., 2018b). To calculate the *PDSI* series, we follow Allen et al., (1998) and apply the Penman-FAO56 equation (denoted as *PET_pm*):

$$PET\_pm = \frac{0.408\Delta(R_n - G) + \gamma\frac{900}{T+273}U_2 \cdot e_s(1 - Rh/100)}{\Delta + \gamma(1 + 0.34U_2)} \quad (1)$$

where *Rn* is the net radiation (can be calculated using surface downwelling/upwelling shortwave/longwave radiation), Δ is the slope of the vapor pressure curve, *G* is the soil heat flux, U_2 is the wind speed (*Ws*) at 2 m above ground level, γ is the psychometric constant, e_s is the saturation vapor pressure at a given air temperature, and *Rh* is the relative humidity. In this study, long-term *PDSI* series over the period 1850–2099 were calculated using the tool provided by the Palmer Drought Severity Index (Jacobi et al., 2013).

According to *PDSI* classification, the severely dry conditions considered as extreme drought in this study are identified using a *PDSI* value less than −3 (the threshold = −3) in a given month. For each decade, the frequency of extreme drought (denoted as *FED*) and its relative change (denoted as *RCFED*) can be further quantified. The change in *RCFED* with warming can be obtained from the statistical value of the linear trend at the grid-box level. Note that we set the baseline period as 2090–2099 instead of 1980–2000 in the decreasing *RCFED* cases. In this way, the *RCFED* values for increasing or decreasing extreme drought cases can be compared with one another (the absolute value for *RCFED* in both increasing and decreasing extreme drought frequency can exceed 100%; refer to brief description in Fig. 2).

2.3. Design of numerical experiments to quantify the sensitivity of extreme drought

Step 1: Eliminating the trend signals

To disentangle different responses of extreme droughts (*PDSI* < −3) to individual meteorological forcing from GCMs in a trend component, as in Zhang et al. (2018), a "detrended" approach was applied. The "detrended" forcing series can be considered as a scenario without the trend signals of climate change. In this study, the "detrended" approach for a given grid box (2000–2099) is expressed as follows:

$$F_{m-detrend,i} = F_{m-sim,i} + \alpha(i_{order} - 2000) \quad (2)$$

where *Fm-sim,i* is the monthly (*temperature, T*) meteorological forcings in year i. *Fm-detrend,i* is the "detrended" monthly forcings in the same year. α is the annual trend for a grid box. The time series, *iorder,* is from 2000 to 2099.

For other meteorological forcings, the "detrended" approach for a given grid box is expressed as follows:

$$F_{y-detrend,i} = F_{y-sim,i} + \alpha(i_{order} - 2000) \quad (3)$$

where *Fy-sim,i* is the annual (*precipitation P; wind speed Ws; relative humidity Rh and net radiation Rn*) meteorological forcings in year i, respectively. *Fy-detrend,i* is the "detrended" annual meteorological forcings in the same year, respectively. α is the annual trend for a grid box. The time series, *iorder,* is from 1980 to 2099.

From above, the monthly "detrended" forcing (*P, Ws, Rh and Sd*) can be generated using:

$$F_{m-\mathrm{det}rend,i} = F_{m-sim,i}\left(\frac{F_{y-\mathrm{det}rend,i}}{F_{y-sim,i}}\right) \quad (4)$$

where *Fm-sim,i* is the projected monthly forcings (*P, Ws, Rh and Sd*) in year i, and *Fm-detrend,i* is the "detrended" monthly meteorological forcings (*P, Ws, Rh and Sd*) in the same year

Step 2: Eliminating the variability signals

To further quantify the different responses of extreme droughts to a single meteorological forcing as a result of a change in variability, a new method for eliminating individual meteorological forcing variability is applied (termed as the "equal variance" approach). Based on the variance of t he baseline period (1980–1999) at the grid-box level, a new series of long-term forcing can be reconstructed using constant variance for each decadal period (i.e., 1850–1859, 1860–1869, … , 2090–2099). Meanwhile, the decadal mean state of the *PDSI* is not modified. Thus, the new series only contains the signals of the trend components (a detailed proof in Appendix A). For a given grid box, the variability (heteroscedasticity) of an individual meteorological forcing from GCMs is eliminated using:

$$F_{\text{y - (equal variance)},i} = k_{decade}(X_{y-sim,i} - \bar{X}_{decade}) + \bar{X}_{decade} \quad (5)$$

where $\bar{X}_{decade}$ is the decadal average of meteorological forcing from GCMs, $X_{y-sim,i}$ is the annual forcing in a given decade in year i, k_{decade} is the correction coefficient of variance and $F_{\text{y - (equal variance)},i}$ is the "equal variance" annual meteorological forcing in the same year *i*. We note that

$$k_{decade} = \frac{Std(X_{y-sim,base})}{Std(X_{y-sim,decade})} \quad (6)$$

where $Std(X_{y-sim,base})$ is the standard deviation of annual meteorological forcing from GCMs over the baseline period and $Std(X_{y-sim,decade})$ is the standard deviation of annual meteorological forcing from GCMs in each decadal period (such as 1850–1859, 1860–1869 … 2080–2089 and 2090–2099).

Subsequently, the monthly "equal variance" forcing can be generated from:

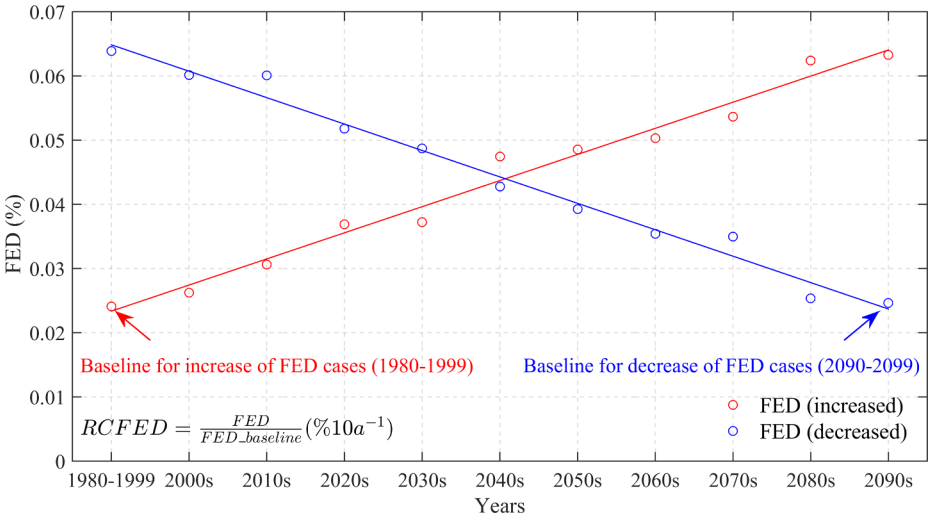

Fig. 2. The two different baseline periods for increasing or decreasing RCFED cases. The baseline period 1980–1999 for the increased RCFED (red line) cases; and the baseline period 2090–2099 for the decreased RCFED cases. (For interpretation of the references to colour in this figure legend, the reader is referred to the web version of this article.)

$$F_{m-(\text{equal variance}),i} = F_{y-(\text{equal variance}),i} \cdot \left(\frac{X_{m-sim,i}}{X_{y-sim,i}} \right) \quad (7)$$

where $X_{m-sim,i}$ is the monthly meteorological forcings from GCMs in year i, and $F_{m-(\text{equal variance}),i}$ is the monthly "equal variance" in meteorological forcings from GCMs in the same year *i*.

2.4. Framework of numerical experiments for attributing the changes in future extreme droughts

To separate different responses (i.e., trend or/and variability components) of the *PDSI* to meteorological forcing from the GCMs and quantify the sensitivity of droughts, we design a baseline case to examine the *PDSI* series when all climatic forcing is free of trends and variability. To this end, we apply the "detrending" technique described in step 1 and then use the "equal variance" approach of step 2 to form a new climatic time series without the long-term climate change signals. It should be emphasized that most climatic variables are generally bounded by zero (e.g., precipitation, wind speed, radiation and relative humidity), and certain climatic variables are further bounded by one (e.g., relative humidity). For these meteorological variables, we first apply "detrending" or "equal variance" to eliminate the trend or variability components. Then, we take the relevant physical constraints into account (no less than zero and/or no larger than one) to avoid unphysical outcomes.

Next, we conduct a series of numerical experiments in which all of the forcing are "detrended" and "equal variance", and the trend signal in a single meteorological variable is used in the *PDSI* estimates. For example, "the precipitation (*P*) trend" case is a numerical experiment in which all meteorological variables are "detrended" and "equal variance", but only the precipitation trend signal is retained. The same approach is also applied to the "temperature (*T*) trend", "wind speed (*Ws*) trend", "net radiation (*Rn*) trend" and "relative humidity (*Rh*) trend" cases. Similarly, we conduct a further series of numerical experiments in which all of the forcings are "detrended" while retaining the variability signal in a single meteorological variable, i.e., the "precipitation (*P*) variability", "temperature (*T*) variability", "wind speed (*Ws*) variability", "net radiation (*Rn*) variability" and "relative humidity (*Rh*) variability" cases. Finally, we release the forcing trend and variability signals in all meteorological variables as the future simulated estimate (denoted as "sim case").

3. Results

3.1. Changes in projected extreme droughts in China

To estimate and reveal the characteristics of future droughts in China, a long-term series of annual *PDSIs* (ensemble mean ± standard) from 1980 to 2099 is presented in Fig. 3a. The overall trend of the *PDSI* indicates a slightly drying trend (-0.04·10a^{-1}) with a widening range of annual *PDSI*. The standard deviation of annual *PDSI* significantly increases for all the 30-year periods (i.e., $STD_{PDSI\_1980\text{-}2009} = 0.16$, $STD_{PDSI\_2010\text{-}2039} = 0.21$, $STD_{PDSI\_2040\text{-}2069} = 0.23$ and $STD_{PDSI\_2070\text{-}2099} = 0.24$). In the end of 21st century, $STD_{PDSI\_2070\text{-}2099}$ is 1.5 times higher than $STD_{PDSI\_1980\text{-}2009}$ (Fig. 3a). According to the conceptual models mentioned above (Fig. 1), the projected drought pattern for the 21st century is characterized by an increase in the drying trend and amplification of drought variability. It is expected that the frequency of extreme drought (*FED*) would increase drastically from the baseline period (i.e., *FED*_baseline = 5.2%) to the end of the 21st century (i.e., *FED*_2090s = 14.8%) (Fig. 3b); and that there would be a strong linear relationship between *FED* and warming signals (i.e., $FED = 0.016\,T + 0.03$, $r = 0.96$). With a slight change in the mean state of drought, the projected extreme drought frequency would dramatically increase in a warmer climate (Trenberth et al., 2003; Liu et al., 2016). To quantify the response of extreme drought to warming, we define an extreme drought rate with warming (denoted as *EDRW* and defined as $\frac{\partial RCFED}{\partial T}$, *unit*: %·K^{-1}), which is the ratio of the change in *RCFED* (unit: %·10a^{-1}) to the decadal change in temperature (unit: K·10a^{-1}). Overall, the projected *RCFED* would increase by approximately 29.3% per Kelvin in China ($EDRW_{\_sim} = 29.3\%\cdot K^{-1}$, Fig. 3c and spatial difference showed in Fig. 7a).

3.2. Quantifying the sensitivity of extreme droughts using PDSI

3.2.1. Designing a baseline case without climate change signals

A series of numerical experiments are performed to quantify the future sensitivity of extreme drought. From there, the probability density function (*PDF*) of *EDRW* $\left(\frac{\partial RCFED}{\partial T}\right)$ is provided from 282 grid-boxes (Fig. 4 and Table 2). According to the baseline case designed in Section 2.4, the trend and variability signals are removed from all meteorological variables. In a sense, it can be regarded as a climate system without long-term climate change signals. In this baseline case, the mean trend of *RCFED* approaches zero and is approximately normally distributed (the blue line in Fig. 4). The average *EDRW* is +1.97%·K^{-1} with a standard deviation of 8.14%·K^{-1}. The new *PDSI* time series can be regarded as a baseline case and serve as a basis for comparison in the following numerical experiments.

3.2.2. Trend components of projected extreme droughts in China

To decompose the sensitivity of extreme droughts into the trend components, the PDF of *EDRW* from the averaged multimodel is shown for each individual numerical experiment. First, we release the trend signals of near-surface temperature and precipitation (i.e., the T trend case and the P trend case). Significant increasing trends for $EDRW_{\_T(trend)}$ ($\mu = 56.90\%\cdot K^{-1}$) and decreasing trends of the same order of magnitude for $EDRW_{\_P(trend)}$ ($\mu = -60.12\%\cdot K^{-1}$), termed "wetting", are shown in Fig. 4a and b, respectively.

Then, we release the trend signal of net radiation and find that a significant increase in $EDRW_{\_Rn(trend)}$ ($\mu = 14.80\%\cdot K^{-1}$) occurs, on average, as much as a quarter of the "warming" contribution to extreme drought. Although a counterintuitive decrease in net radiation was observed worldwide in the 20th century under global warming (termed "global dimming"), a rapid increase in net radiation commenced after the 1990 s (Wild et al., 2005; Trenberth and Fasullo, 2009) in response to a sharp increase in temperature (termed "global brightening") from the early 21st century.

To quantify the sensitivity of extreme drought in terms of trend components, we investigate the remaining two meteorological variables (i.e., wind speed and relative humidity) in separate manner. By releasing the wind speed trend (wind speed trend case), the PDF of $EDRW_{\_Ws(trend)}$ is nearly unchanged according to average and standard deviation ($\mu = 0.64\%\cdot K^{-1}$, $\sigma = 7.86\%\cdot K^{-1}$). A decrease in relative humidity has been widely confirmed (Lorenz et al., 2010; Byrne et al., 2016). As expected, by releasing the relative humidity trend, $EDRW_{\_Rh(trend)}$ exhibits a minor increasing trend ($\mu = 4.61\%\cdot K^{-1}$), with a slightly larger standard deviation ($\sigma = 9.79\%\cdot K^{-1}$). The projected increase in net radiation and decrease in relative humidity in a warmer climate could result in higher atmospheric evaporative demand and hence more extreme droughts.

3.2.3. Variability components of projected extreme droughts in China

The same framework with a series of numerical experiments was applied to quantify the sensitivity of extreme drought caused by the inter-decadal change in the variability of climate variables. *EDRW* changes little in its standard deviation and average values when the variability of temperature, net radiation, wind speed and relative humidity are considered, respectively (Fig. 4e, g and h). However, the averaged $EDRW_{\_P(variability)}$ ($\mu = 8.23\%\cdot K^{-1}$) increases remarkably (Fig. 4f). This means that the projected frequency of extreme drought is unaffected by the change in the

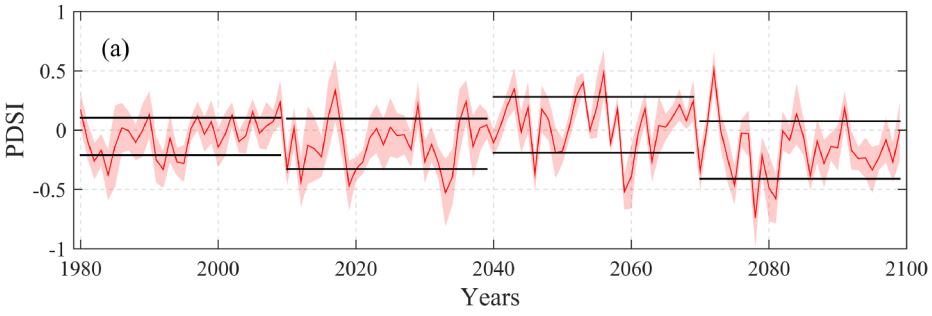

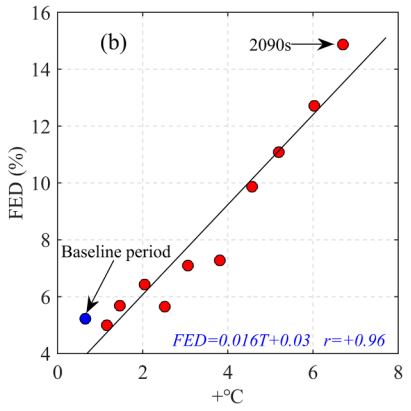

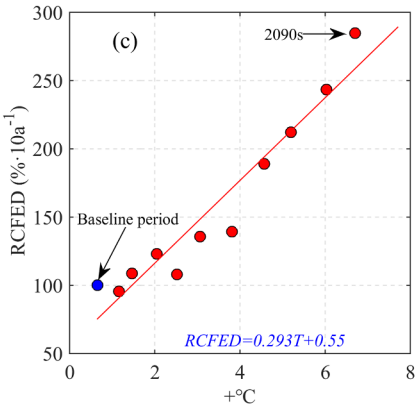

Fig. 3. Changes in droughts and interdecadal changes in the frequency of extreme drought across China from 1980 to the end of the 21st century: (a) the time series of annual *PDSI*; the shaded range is σ for seven GCMs, and the horizontal line (black) is the mean ± standard of the ensemble mean for each 30-year period (1980–2009; 2010–2039; 2040–2069; 2070–2099); (b) the frequency of extreme drought (denoted *FED*) with global warming relative to the preindustrial level on the decadal scale; (c) relative changes in *FED* (denoted *RCFED*).

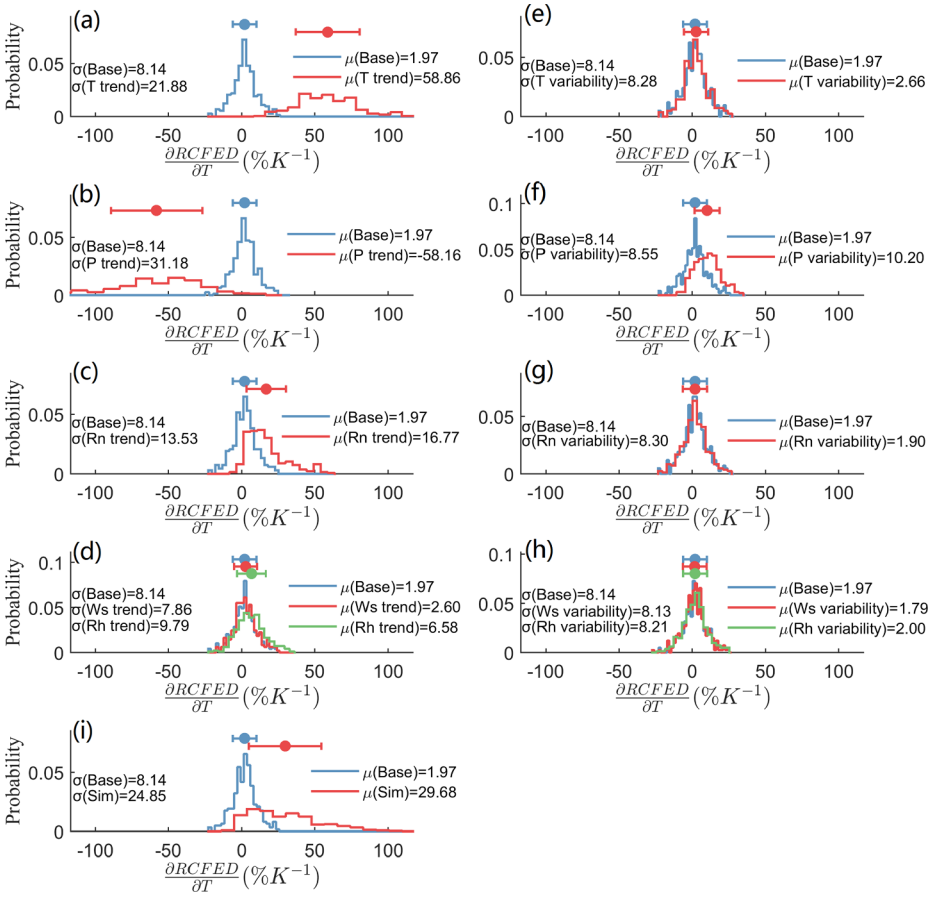

Fig. 4. Sensitivity of changes in future extreme droughts to different driving factors across China based on a series of numerical experiments. The PDF of *EDRW* is eliminated trend and variability signals (mentioned in Section 2) for all variables but the trend components, i.e., a) temperature (*T*) trend case; b) precipitation (*P*) trend case; c) net radiation (*Rn*) trend case; d) wind speed (*Ws*) /relative humidity (*Rh*) trend case. Variability components: e) temperature (*T*) variability case; f) precipitation (*P*) variability case; g) net radiation (*Rn*) variability case); h) wind speed (*Ws*)/relative humidity (*Rh*) variability case; i) simulated (Sim) case: trend and variability, in all meteorological variables are maintained. The blue line is the *PDF* of *EDRW* from which the trend and variability signals for all variables are eliminated, it represents the baseline (Base) case. The horizontal lines indicate the mean ± standard deviation from 282 grid boxes in the relevant numerical experiment. (For interpretation of the references to colour in this figure legend, the reader is referred to the web version of this article.)

variability of climate variables except precipitation. Note that $EDRW_{P(variability)}$ is very close to the ratio of increase in extreme precipitation to warming of the Clausius-Clapeyron relation (~7%·K^{-1}) (Utsumi et al., 2011; Berg et al., 2013; Fischer and Knutti, 2016). Previous studies emphasized that the amplification of variability in interannual precipitation could increase the risk of flood (Wang et al., 2016; Swain et al., 2018). The projected amplification of precipitation variability reported here could also markedly increase the risk of extreme drought (He and Li, 2018; Swain

Table 2
Summary of averaged *RCFED* with climate warming in different numerical experiments (unit: %·K^{-1}). Note that the column represents the contribution of each (and all) meteorological variable(s) (trend and variability component) by taking the difference between each case and the baseline case in the relevant numerical experiment.

	T (only)	P (only)	Rn (only)	Ws (only)	Rh (only)	All
Trend components	56.90	−60.12	14.80	0.64	4.61	16.83
Variability components	0.70	+8.23	−0.07	−0.17	0.04	8.73
Total	57.60	−51.89	14.73	0.47	4.65	25.56

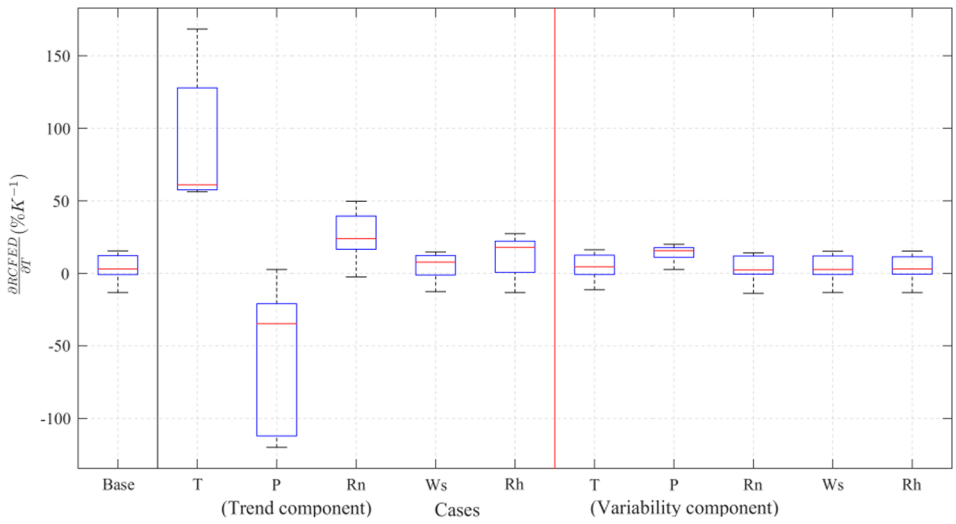

Fig. 5. Projected uncertainty of multiple climate models using box plot for each numerical experiments over China.

et al., 2018). These outcomes suggest that the change in extreme drought is not only due to temperature, precipitation, net radiation and relative humidity trends but also partly to an increase in precipitation variability. Taking all these contributing factors into account, the projected relative change in extreme drought frequency per Kelvin ($EDRW_{sim}$) could hit an average of 27.71%·K^{-1}, very close to the summed averaged contribution from all simulation experiments (sum of contribution = 25.56%·K^{-1}). Nonetheless, inter-model uncertainties remain high, particularly for precipitation (i.e., "wetting") and temperature (i.e., "warming") projections (Fig. 5).

3.3. Spatial pattern of projected extreme droughts in China

It is widely anticipated that the near-surface temperature would increase strongly in the high-latitude regions but moderately in the low-latitude regions under climate change (IPCC, 2013). To examine whether this would have any implications for extreme droughts in different latitude zones of China, we apply our framework and numerical experiments to quantify the sensitivity of extreme droughts for a range of latitude zones. Here, we focus on latitude zones with greater than 15 grid boxes so that the statistics are more robust (Fig. 6a). First, the five

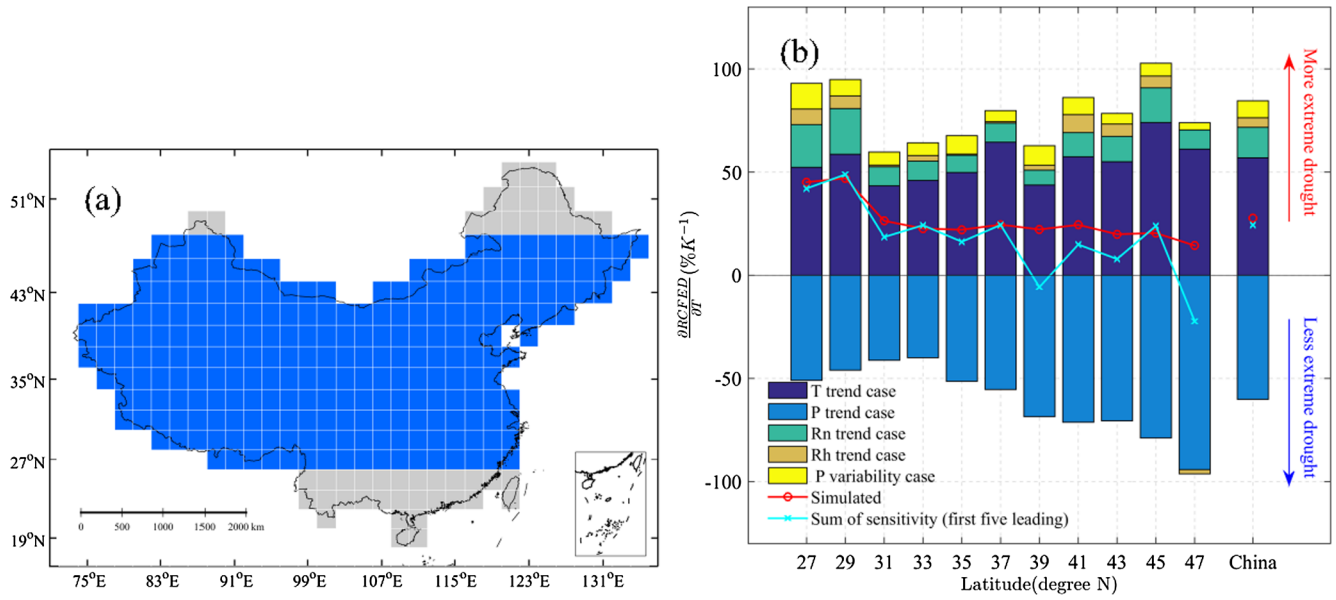

Fig. 6. Regional (latitudinal) sensitivity of extreme droughts with climate warming for the five leading components: a) a total of 236 of 282 grid boxes are selected over 26°-48° *N* of China, and in the same latitude, at least 15 grid boxes are included; b) averaged sensitivity for different latitudinal zones.

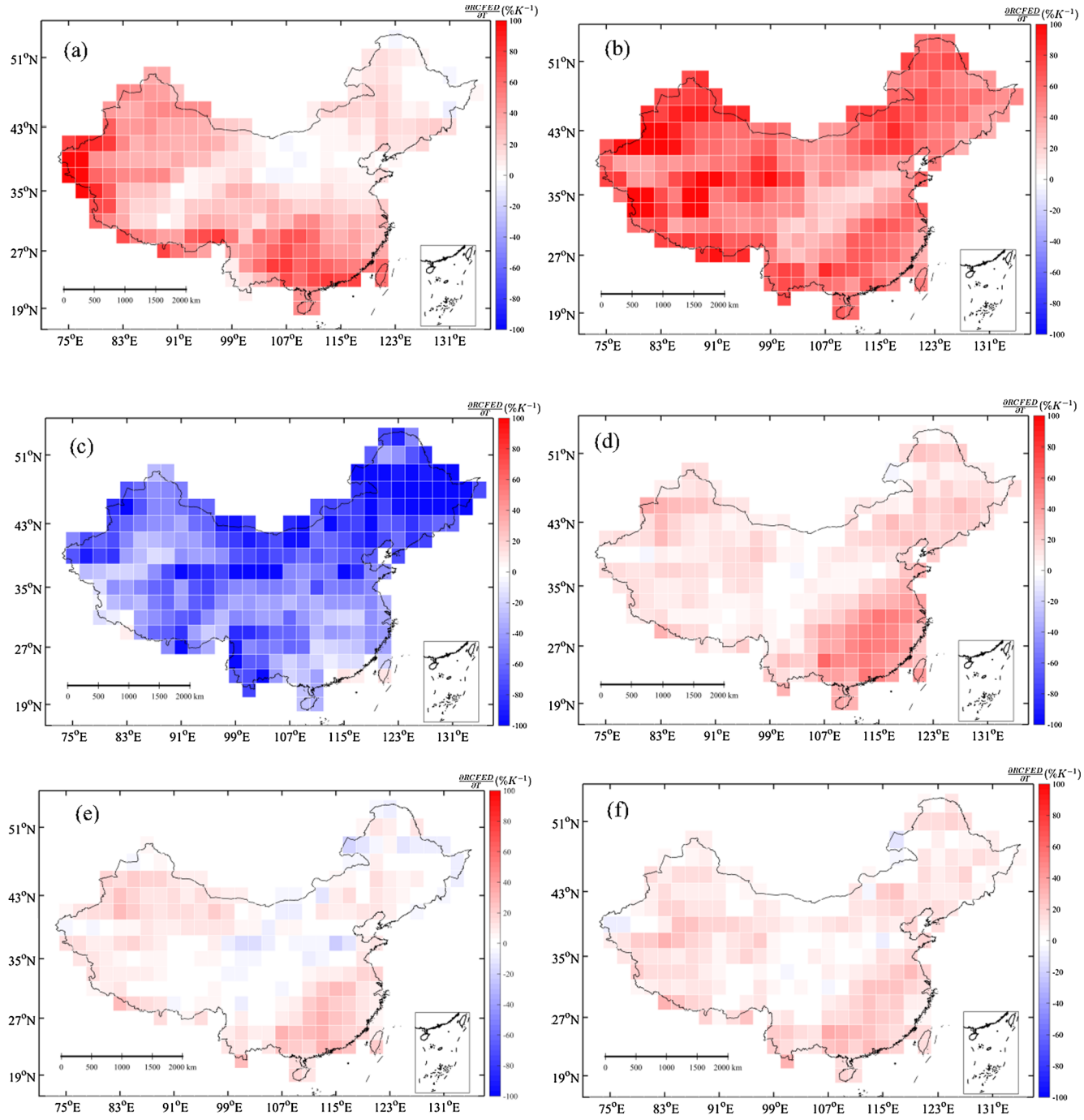

Fig. 7. Changes in multi-model ensemble mean RCFED for per degree of warming in numerical experiments. a) future estimate (sim case); b) T trend case; c) P trend case; d) Rn trend case; e) Rh trend case; f) P variability case.

leading components of extreme drought (i.e., temperature trend, precipitation trend, net radiation trend, relative humidity trend and precipitation variability) are evaluated on a regional (i.e., latitudinal) scale. Whilst temperature rise is the primary factor of more extreme droughts in various regions, it could be partly (in low-latitude regions) or completely offset (in high-latitude regions) by "wetting" (Fig. 7b and c). When the other three main factors (i.e., the increase in net radiation, decrease in relative humidity and amplification of precipitation variability) are added (Fig. 7e-f), the sum of $EDRW_{\_T(Trend)}$, $EDRW_{\_Rn(Trend)}$, $EDRW_{\_Rh(Trend)}$ and $EDRW_{\_P(Variability)}$ could reach 53.2%·K^{-1} in the mid-latitude region (31°–33°*N*) and more than 80%·K^{-1} in the low- (or high-) latitude regions (Fig. 6b). According to the projected precipitation trend, we found that $EDRW_{\_P(Trend)}$ declines with increasing latitude (approximately $-50\%\cdot K^{-1}$ in a low-latitude zone (26°-34°*N*) and $-94.3\%\cdot K^{-1}$ in a high-latitude zone (46°-48°*N*), Fig. 7c). Projected *EDRW_sim* and the sum of *EDRW* from the first five leading components (*EDRW_sum*) are significantly higher in the high-latitude regions than those in the low-latitude regions (see the red line for the simulation outcome and the blue line for the sum of sensitivity in Fig. 6b). The projected change in precipitation with global warming would dominate the spatial pattern of future extreme drought risk (correlation coefficient between $EDRW_{\_P(Trend)}$ and $EDRW_{\_Sim}$ = 0.56 at regional scales).

4. Summary and discussion

This study emerged from the lack of systematic understanding about

the contributing factors towards the projected increase in extreme droughts in many regions under global warming. To investigate the attribution of the change in extreme drought frequency, we selected China as the study area and assessed the change in future extreme drought frequency using *PDSI* based on a set of outputs from seven CMIP5 GCMs under the concentration pathway scenario RCP8.5. Based on the ensemble mean, annual *PDSI* would slightly decrease (-0.04·10a^{-1}) over the period 1980–2099. By contrast, the risk of extreme drought would increase drastically per Kelvin.

To attribute the increase in extreme droughts with warming, we designed a series of numerical experiments, including a baseline case without climate change at the grid-box scale (all meteorological variables free of trends and variability) and additional ten separate cases that covered the individual trend or variability in a meteorological variable (Fig. 3). To quantify the difference response to warming, we further defined an extreme drought rate with warming to determine the possible influence of climate change on extreme drought in a warmer future climate.

The first two leading factors of the change in extreme drought frequency are “warming” and “wetting”, as noted in Conceptual Model 1 (Fig. 1b). Theoretically, the precipitation increases (i.e., “wetting”) about 1–3% per degree of warming because of the response of the increased atmospheric radiative energy (Held and Soden, 2006; Naumann et al., 2018), and the sensitivity of “wetting” to extreme drought ($EDRW_{P(trend)} = -60.12\%\cdot K^{-1}$) is enough to offset the increase in extreme drought caused by warming ($EDRW_{T(trend)} = +56.90\%\cdot K^{-1}$) for all China.

In addition, the increase in net radiation and the decrease in relative humidity can result in more extreme drought ($EDRW_{Rn(trend)}$: $\mu = 14.8\%\cdot K^{-1}$ and $EDRW_{Rh(trend)}$: $\mu = 4.61\%\cdot K^{-1}$), as also noted in Conceptual Model 1 (Fig. 1b). In a warming climate, precipitation tends towards the temporal pattern of longer nonprecipitation periods and frequent extreme heavy precipitation (Trenberth et al., 2003). The amplification of precipitation variability can result in more extreme drought ($\mu(EDRW_{P(variability)}) = 8.23\%\cdot K^{-1}$), as noted in Conceptual Model 2 (Fig. 1c). Interestingly, $EDRW_{P(variability)}$ is close to the ratio of change in extreme precipitation in response to warming according to the Clausius-Clapeyron relation ($\sim 7\%\cdot K^{-1}$). However, intermodel uncertainties remain high, particularly in precipitation and temperature projections.

We further apply the same framework to quantify the sensitivity of extreme droughts at latitudinal (regional) scales. We found that the projected extreme drought ($EDRW_{sim}$) and the sum of sensitivity for the first five leading components ($EDRW_{sum}$) are both consistently higher in high-latitude than low-latitude regions, which is mainly due to the spatial pattern of the precipitation trend. This outcome suggests that extreme drought frequency in low-latitude China will be substantially higher per degree of warming in the future.

Acknowledgements:

This study was financially supported by the National Key Research and Development Program of China (2016YFA0602402 and 2016YFC0401401), the Key Research Program of the Chinese Academy of Sciences (ZDRW-ZS-2017-3-1, ZDRW-ZS-2019-3), the CAS Pioneer Hundred Talents Program (Fubao Sun) and the China Postdoctoral Science Foundation (2018M640174).

Appendix A

A proof of the unchangeability and homoscedasticity when the variability signals was eliminated using “equal-variance” approach in this study.

The unchangeability of the decadal average for $F_{y-(\text{equal variance})}$ is expressed as follows:

$$\bar{F}_{y-(\text{equal variance}),decade} = \frac{k_{decade}\sum_{i=j}^{j+9}(X_{y-sim,i} - \bar{X}_{decade})}{10} + \bar{X}_{decade}$$
$$= k_{decade}(\bar{X}_{decade} - \bar{X}_{decade}) + \bar{X}_{decade} = \bar{X}_{decade}$$

where j is the beginning year of each decade, and $j = 1850, 1860, \cdots 2090$. $\bar{X}_{decade}$ is the decadal average of meteorological forcing from GCMs, $X_{y-sim,i}$ is the annual forcing in a given decade in year i, k_{decade} is the correction coefficient of variance and $F_{y\text{ - equal variance},decade}$ is the “equal variance” annual meteorological forcing in the same decade.

The homoscedasticity of $F_{y-(\text{equal variance})}$ can be derived as follows:

$$Std(F_{y-(\text{equal variance}),decade}) = Std[k_{decade}(X_i - \bar{X}_{decade}) + \bar{X}_{decade}]$$
$$= \sqrt{\frac{\sum[k_{decade}X_{y-sim,i} + (1-k_{decade})\bar{X}_{decade}]^2}{10-1}} = k_{decade}\sqrt{\frac{\sum[X_{y-sim,i} - \bar{X}_{decade}]^2}{9}}$$
$$= \frac{Std(X_{y-sim,base})}{Std(X_{y-sim,decade})}\cdot Std(X_{y-sim,decade}) = Std(X_{y-sim,base})$$

where $X_{y-sim,base}$ is the average of meteorological forcing from GCMs in the baseline period 1980–1999.

References

Aghakouchak, A., Cheng, L., Mazdiyasni, O., Farahmand, A., 2015. Global warming and changes in risk of concurrent climate extremes: insights from the 2014 California drought. Geophys. Res. Lett. 41, 8847–8852. https://doi.org/10.1002/2014GL062308.

Allen, R., Pereira, L., Raes, D., Smith, M., 1998. Crop evapotranspiration guidelines for computing crop water requirements, FAO Irrig. Drain. Pap. 56, Food and Agric. Organ. of the U. N., Rome.

Berg, P., Moseley, C., Haerter, J.O., 2013. Strong increase in convective precipitation in response to higher temperatures. Nat. Geosci. 6, 181–185. https://doi.org/10.1038/ngeo1731.

Byrne, M., O'Gorman, P., 2016. Understanding decreases in land relative humidity with global warming: Conceptual model and GCM simulations. J. Clim. 29 (24), 9045–9061. https://doi.org/10.1175/JCLI-D-16-0351.

Chen, H., Sun, J., 2015. Changes in climate extreme events in china associated with warming. Int. J. Climatol 35 (10), 2735–2751. https://doi.org/10.1002/joc.4168.

Chen, T., et al., 2017. Robust drying and wetting trends are found in regions based on köppen climate classifications over china. J. Geophys. Res. 122 (8), 4228–4237. https://doi.org/10.1002/2016JD026168.

Cook, B.I., Ault, T.R., Smerdon, J.E., 2015. Unprecedented 21st century drought risk in the American Southwest and Central Plains. Sci. Adv. 1 (1), e1400082. https://doi.org/10.1126/sciadv.1400082.

Dai, A., Zhao, T.B., 2016. Uncertainties in historical changes and future projections of drought, part I: estimates of historical drought changes. Clim. Change 1–15. https://doi.org/10.1007/s10584-016-1705-2.

Diffenbaugh, N.S., Swain, D.L., Touma, D., 2015. Anthropogenic warming has increased drought risk in California. Proc. Natl. Acad. Sci. 112 (13), 3931–3936. https://doi.org/10.1073/pnas.1422385112.

Fischer, E.M., Knutti, R., 2016. Observed heavy precipitation increase confirms theory and early models. Nat. Clim. Chang. 6 (11), 986–991. https://doi.org/10.1038/nclimate3110.

He, C., Li, T., 2018. Does global warming amplify interannual climate variability? Clim. Dyn. 1–18.

Held, I.M., Soden, B.J., 2006. Robust responses of the hydrological cycle to global warming. J. Clim. 19 (21), 5686–5699. https://doi.org/10.1175/JCLI3990.1.

Herrera-Estrada, J.E., Satoh, Y., Sheffield, J., 2017. Spatiotemporal dynamics of global drought. Geophys. Res. Lett. 44 (5), 2254–2263. https://doi.org/10.1002/2016GL071768.

IPCC: Climate Change, 2013. The Physical Science Basis, Contribution of Working Group I

to the Fifth Assessment Report of the Intergovernmental Panel on Climate Change. Cambridge Univ. Press, Cambridge, U. K.
Jacobi, J., Perrone, D., Duncan, L.L., Hornberger, G., 2013. A tool for calculating the Palmer drought indices. Water Resour. Res. 49, 6086–6089. https://doi.org/10.1002/wrcr.20342.
Kauffman, G.J., Vonck, K.J., 2011. Frequency and intensity of extreme drought in the Delaware Basin, 1600–2002. Water Resour. Res. 47 (5), W05521. https://doi.org/10.1029/2009WR008821.
Kiem, A.S., et al., 2016. Natural hazards in Australia: droughts. Clim. Change 139 (1), 37–54. https://doi.org/10.1007/s10584-016-1798-7.
Lehner, F., Coats, S., Stocker, T.F., Pendergrass, A.G., Sanderson, B.M., Raible, C.C., Smerdon, J.E., 2017. Projected drought risk in 1.5 °C and 2 °C warmer climates. Geophys. Res. Lett. 44 (14), 7419–7428. https://doi.org/10.1002/2017GL074117.
Liu, W.B., Wang, L., Zhou, J., Li, Y.Z., Sun, F.B., Fu, G.B., Li, X.P., Sang, Y.-F., 2016. A worldwide evaluation of basin-scale evapotranspiration estimates against the water balance method. J. Hydrol. 538, 82–95.
Liu, W., et al., 2018a. Global freshwater availability below normal conditions and population impact under 1.5 and 2 °C stabilization scenarios. Geophys. Res. Lett. https://doi.org/10.1029/2018GL078789.
Liu, W., et al., 2018b. Global drought and severe drought affected population in 1.5°C and 2°C warmer worlds. Earth. Syst. Dyn. 9 (1), 267–283. https://doi.org/10.5194/esd-9-267-2018.
Lorenz, D.J., DeWeaver, E.T., D. J. Vimont.,, 2010. Evaporation change and global warming: the role of net radiation and relative humidity. J. Geophys. Res. 115, D20118. https://doi.org/10.1029/2010JD013949.
Mishra, A.K., Singh, V.P., 2010. A review of drought concepts. J. Hydrol. 391 (1–2), 202–216. https://doi.org/10.1016/j.jhydrol.2010.07.012.
Naumann, G., et al., 2018. Global changes in drought conditions under different levels of warming. Geophys. Res. Lett. 45 (7), 3285–3296. https://doi.org/10.1002/2017GL076521.
Palmer, W.C., 1965. Meteorological Drought. US Department of Commerce, Weather Bureau, Washington, D. C.
Prudhomme, C., et al., 2014. Hydrological droughts in the 21st century, hotspots and uncertainties from a global multimodel ensemble experiment. Proc. Natl. Acad. Sci. 111 (9), 3262–3267. https://doi.org/10.1073/pnas.1222473110.
Qiu, J., 2010. China drought highlights future climate threats. Nature 465, 142–143. https://doi.org/10.1038/465142a.
Sheffield, J., Wood, E.F., Roderick, M.L., 2012. Little change in global drought over the past 60 years. Nature 491 (435–438). https://doi.org/10.1038/nature11575.
Seager, R., Naik, N., Vogel, L., 2012. Does global warming cause intensified interannual hydroclimate variability? J. Clim. 25, 3355–3372. https://doi.org/10.1175/JCLI-D-11-00363.1.
Swain, D.L., Langenbrunner, B., Neelin, J.D., Hall, A., 2018. Increasing precipitation volatility in twenty-first-century California. Nat. Clim. Chang. 8 (5), 427. https://doi.org/10.1038/s41558-018-0140-y.
Trenberth, K.E., Dai, A., Rasmussen, R.M., Parsons, D.B., 2003. The changing character of precipitation. Bull. Am. Meteorol. Soc. 84, 120–1217. https://doi.org/10.1175/BAMS-84-9-1205.
Trenberth, K.E., Fasullo, J.T., 2009. Global warming due to increasing absorbed solar radiation. Geophys. Res. Lett. 36, L07706. https://doi.org/10.1029/2009GL037527.
Utsumi, N., Seto, S., Kanae, S., Maeda, E.E., Oki, T., 2011. Does higher surface temperature intensify extreme precipitation? Geophys. Res. Lett. 38, L16708. https://doi.org/10.1029/2011GL048426.
Van Dijk, A.I., Beck, H.E., Crosbie, R.S., de Jeu, R.A., Liu, Y.Y., Podger, G.M., Viney, N.R., 2013. The Millennium Drought in southeast Australia (2001–2009): Natural and human causes and implications for water resources, ecosystems, economy, and society. Water Resour. Res 49 (2), 1040–1057. https://doi.org/10.1002/wrcr.20123.
Vicente-serrano, S.M., Beguería, S., López moreno, J.I., 2010. A multiscalar drought index sensitive to global warming: the standardized precipitation evapotranspiration index. J. Clim. 23 (7), 1696–1718. https://doi.org/10.1175/2009JCLI2909.1.
Wang, W., et al., 2015. Drought severity change in china during 1961–2012 indicated by SPI and SPEI. Nat. Hazards 75 (3), 2437–2451. https://doi.org/10.1007/s11069-014-1436-5.
Wang, S.Y.S., Zhao, L., Gillies, R.R., 2016. Synoptic and quantitative attributions of the extreme precipitation leading to the August 2016 Louisiana flood. Geophys. Res. Lett 43 (22), 11805–11814. https://doi.org/10.1002/2016GL071460.
Wetherald, R.T., 2009. Changes of variability in response to increasing greenhouse gases. Part II: hydrology. J. Clim. 22 (22), 6089–6103. https://doi.org/10.1175/2009JCLI2834.1.
Wild, M., et al., 2005. From dimming to brightening: decadal changes in surface solar radiation. Science 308, 847–850. https://doi.org/10.1126/science.1103215.
Zhang, J., Chen, H., Zhang, Q., 2018. Extreme drought in the recent two decades in northern china resulting from eurasian warming. Clim. Dyn. 6, 1–18.
Zhao, T., Dai, A., 2016. Uncertainties in historical changes and future projections of drought. Part II: model-simulated historical and future drought changes. Clim. Change. 144 (3), 535–548. https://doi.org/10.1007/s10584-016-1742-x.
Zou, X., Zhai, P., Zhang, Q., 2005. Variations in droughts over China:1951–2003. Geophys. Res. Lett. 32, L04707. https://doi.org/10.1029/2004GL021853.